Ecotoxicology and Environmental Safety 264 (2023) 115470

Contents lists available at ScienceDirect

Ecotoxicology and Environmental Safety

journal homepage: www.elsevier.com/locate/ecoenv

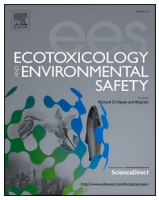

A family of kojic acid derivatives aimed to remediation of Pb^{2+} and Cd^{2+}

Rosita Cappai [a,b,*], Alessandra Fantasia [a,b], Giampaolo Barone [c], Massimiliano F. Peana [a], Alessio Pelucelli [a], Serenella Medici [a], Guido Crisponi [b], Valeria M. Nurchi [b], M. Antonietta Zoroddu [a]

[a] Dipartimento di Scienze Chimiche, Fisiche, Matematiche e Naturali, Università di Sassari, via Vienna 2, 07100 Sassari, Italy
[b] Dipartimento di Scienze della Vita e dell'Ambiente, Università di Cagliari, Cittadella Universitaria, Monserrato, 09042 Cagliari, Italy
[c] Dipartimento di Scienze Biologiche, Chimiche e Farmaceutiche, Università di Palermo, Viale delle Scienze, Edificio 17, 90128 Palermo, Italy

ARTICLE INFO

Editor: Mohamed Abdel-Daim

Keywords:
Kojic acid
Cadmium
Lead
Remediation
Complexation
Environmental chemistry

ABSTRACT

The present work analyzes the complex formation ability towards Pb^{2+} and Cd^{2+} of a series of kojic acid derivatives that join the chelating properties of the pyrone molecules and those of polyamines, with the aim of evaluating how the different effects of oxygen and nitrogen coordinating groups act on the stability of metal complexes. Experimental research is carried out using potentiometric and spectrophotometric techniques supported by ^{1}H and ^{13}C NMR spectroscopy and DFT calculations. Actually, a different coordination mechanism toward Pb^{2+} and Cd^{2+} was proved: in the case of Pb^{2+}, coordination takes place exclusively *via* the oxygen atoms, while the contribute of the nitrogen atoms appears relevant in the case of Cd^{2+}. Lead complexes of all the studied ligands are characterized by significantly stronger stability than those of cadmium. Finally, on the basis of the measured complex formation stabilities, some of the proposed molecules seems promising effective ligands for lead and cadmium ion decorporation from polluted soils or waste waters.

1. Introduction

Lead and cadmium, according to the US Agency for Toxic Substances & Disease Registry (ATSDR) (ATSDR, 2022) are respectively the second and the seventh in the list of the substances that "cause the most significant problems to human health for their toxicity and potential for human exposure" (Crisponi and Nurchi, 2015). This priority list is not a list of "most toxic" substances, but rather a prioritization of substances based on a combination of their frequency, toxicity, and potential for human exposure (ATSDR, 2022). Despite many national and supranational governments, based on the awareness of their toxicity, have banned their use and their release, the toxicological relevance of these two metal ions is always significant. The heavy metal ions are classified as non-biodegradable pollutants, compounds not decomposed or broken down, and thus persistent and able to accumulate in waters, soils and food chain (Cantu et al., 2019), (Nurchi et al., 2020). The use of lead and cadmium is historically different (the use of lead dates back to Bronze Age while that of cadmium to the second half of the XIX century) as well as their chemical features, the mechanism of their toxicity and the requirements of the chelating agents for their removal from human organism and from polluted environmental sites. Complete toxicological profiles for lead and cadmium are provided by ATSDR, for the first one updated to 2020 (ATSDR, 2020) and for the second updated to 2012 (ATSDR, 2012), together with the main information on chemical and physical properties, production, use, environmental fate, regulations and guidelines. Information on the coordination properties of these two metal ions can be found in recent reviews (Bjørklund et al., 2019), (Cappai et al., 2018), (Crisponi and Nurchi, 2015), (Peana et al., 2021), (Remelli et al., 2016).

In a recent paper (Nurchi et al., 2020) we thoroughly discussed on soil remediation methods, and on soil washing technology with the use of chelating agents as possible extracting ligands of the polluting metal ions. In particular, we proposed a method for the preliminary screening among various potential ligands toward target metal ions, which was applied, as an example, to several aminopolycarboxylic acids largely used in soil remediation thanks to their biodegradability.

Recalling the *hard–soft* properties (Pearson, 1963) of these two metal ions, Cd^{2+} (group 12 in the Periodic Table of Elements) is classified as a *soft* metal ion, preferring coordination by ligands characterized by soft groups (R_2S, RSH, and RS), even if coordination with oxygen and nitrogen atoms is frequently found. On the contrary, Pb^{2+} (group 14) is classified as an intermediate metal ion, preferentially coordinated by

* Corresponding author at: Dipartimento di Scienze Chimiche, Fisiche, Matematiche e Naturali, Università di Sassari, via Vienna 2, 07100 Sassari, Italy.
E-mail address: rcappai1@uniss.it (R. Cappai).

https://doi.org/10.1016/j.ecoenv.2023.115470
Received 28 June 2023; Received in revised form 28 August 2023; Accepted 10 September 2023
Available online 14 September 2023

amino groups, though the interaction with hard oxygen groups and soft sulfur groups can be found in many complexes.

It has to be considered that metal may be present in a specific form depending on concentration, solubility, pH and (ionic) medium (Nurchi et al., 2021). Therefore, complexation studies turn out to be crucial and propaedeutic for many application fields, such as remediation, prediction of metal transport and fate in the design of method with the aim of sequestering a toxic metal from natural systems (Cardiano et al., 2016), (Irto et al., 2020), (Irto et al., 2019).

To enquire on the different effect of oxygen and nitrogen coordinating groups on the stability of Pb^{2+} and Cd^{2+} complexes, the present work analyzes the complex formation ability of a series of kojic acid derivatives (Fig. 1) towards Pb^{2+} and Cd^{2+}, using potentiometry and spectrophotometry supported by ^{1}H and ^{13}C NMR spectroscopy and DFT calculations. The proposed molecules join the chelating properties of the hydroxypyrone molecules (vicinal carbonyl and O^{-} groups) and those of polyamines (ethylenediamine (en), 1,3-diaminopropane (dpa), 1,4-diaminobutane (dba) and 2,2′,2″-triaminotriethyllamine (tren)) (Nurchi et al., 2019a). These ligands show an extremely high similarity with some of the aminopolycarboxylic acids previously evaluated (Nurchi et al., 2020), as can be argued from the comparison of the structures reported in Fig. S1.

In the frame of our research on chelating agents for the treatment of iron overload diseases, we designed, synthesized and characterized a number of kojic acid derivatives, based on the strong coordinating ability of the hydroxypyrone molecule, and on the lack of toxicity of kojic acid, a molecule in wide use in food industry and in cosmetics. Peculiarity of the kojic acid moiety are the strong UV spectral variations connected to its deprotonation, which can allow to distinguish the effects of oxygen and nitrogen coordinating group.

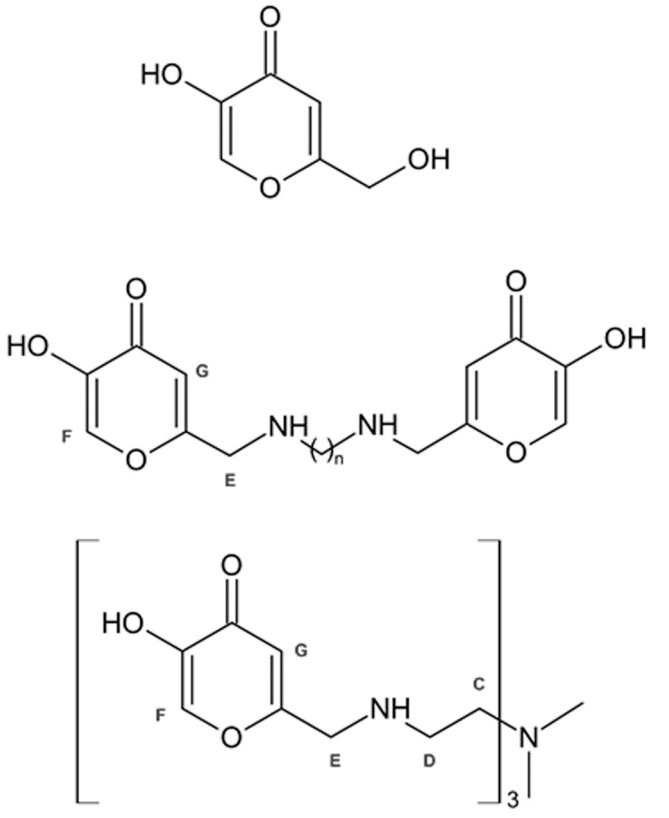

Fig. 1. Ligand structures top): kojic acid; middle): S ligands where n = 2 in S2, n = 3 in S3 and n = 4 in S4; bottom): SC ligand.

2. Materials and methods

2.1. Chemicals and materials

1 mM ligand solutions were prepared by weighing the solid compounds previously synthetized according to literature methods (Nurchi et al., 2019b), (Nurchi et al., 2018). $CdCl_2$ and $Pb(NO_3)_2$ salts, purchased from Sigma Aldrich, were used without any further purification. The metal solutions were prepared by weighing salts, acidified with a stoichiometric amount of HCl and HNO_3 to prevent hydrolysis and standardized by EDTA titration (Buglyó et al., 2015), obtaining 0.0085(1) M for $CdCl_2$ and 0.0102(1) M for $Pb(NO_3)_2$. HCl, HNO_3 and KOH, purchased from Sigma Aldrich, were standardized by sodium carbonate and potassium hydrogen phthalate, respectively. To avoid the carbonation process of KOH titrant solution, soda lime traps were used. KCl and KNO_3 ionic medium aqueous solutions were prepared by weighing the Sigma Aldrich salts. All solutions were prepared using grade A glassware and ultrapure water (conductivity < 0.1 μS).

2.2. Instrumentation and procedures

2.2.1. Potentiometry and spectrophotometry

The complex formation equilibria were studied by combined potentiometric-UV spectrophotometric titrations at 1:1, 1:2 and 1:3 metal:ligand molar ratios (5.0×10^{-4} M ligand concentration) in thermostatic glass cell (25 °C), 0.1 M ionic strength, under magnetic stirring and argon atmosphere to avoid the presence of $CO_{2(g)}$. A combined glass electrode (dEcotrode plus Metrohm) was connected to 888 Titrando (Metrohm AG, Herisau, Switzerland). The electrode was daily calibrated for hydrogen ion concentration *via* HCl standard titration with NaOH in the used experimental conditions, and data processed with Gran's method (Gran, 1952) for determining the electrode potential (E_0), the daily NaOH concentration and the ionic product of water (pK_w). The automatic potentiometric titrations were run using Methrohm TiAMO 1.2 software capable of handling up to 8 μL of titrant additions ($\pm$ 0.001 mL) and e.m.f. measurement ($\pm$ 0.15 mV). Spectrophotometric titrations were carried out with 0.2 cm fiber optic dip probe connected to a Varian Cary 60 Agilent UV–vis spectrophotometer by means of the Varian Cary WinUV software for recording absorbance values (A) in the wavelength range between 200 and 400 nm. The combined potentiometric-spectrophotometric titrations were carried out from pH ~ 2 to ~ 10 according to the formation of insoluble species. Potentiometric and spectrophotometric data were processed using the HyperQuad and HypSpec programs (Frassineti et al., 1995), (Gans et al., 1996), respectively for the optimization of the stability constants. Furthermore, HypSpec program allows the calculation of absorptivity spectra of the involved absorbing species. Log β_{pqr} values refer to the overall equilibria $pM + qH + rL \rightleftarrows M_pH_qL_r$ (electrical charges omitted). L indicates the completely deprotonated form of the ligands. The following hydrolysis constants were assumed for the calculations (Baes and Mesmer, 1976): $[Cd(OH)]^{+}$ ($\log\beta_{1-1} = -10.15$), $Cd(OH)_2$ ($\log\beta_{1-2} = -20.51$), $[Cd(OH)_3]^{-}$ ($\log\beta_{1-3} = -33.33$), $[Cd(OH)_4]^{2-}$ ($\log\beta_{1-4} = -47.39$), $[Cd_2(OH)]^{3+}$ ($\log\beta_{2-1} = -9.25$), $[Cd_4(OH)_4]^{4+}$ ($\log\beta_{4-4} = -32.42$); $[Pb(OH)]^{+}$ ($\log\beta_{1-1} = -7.85$), $Pb(OH)_2$ ($\log\beta_{1-2} = -17.17$), $[Pb(OH)_3]^{-}$ ($\log\beta_{1-3} = -28.09$) $[Pb_2(OH)]^{3+}$ ($\log\beta_{2-1} = -5.71$), $[Pb_3(OH)_4]^{2+}$ ($\log\beta_{3-4} = -23.66$), $[Pb_4(OH)_4]^{4+}$ ($\log\beta_{4-4} = -20.39$), $[Pb_6(OH)_8]^{4+}$ ($\log\beta_{6-8} = -43.36$).

2.2.2. NMR spectroscopy

NMR experiments were performed at 25 °C on a Bruker Ascend™ 400 MHz spectrometer equipped with a 5 mm automated tuning and matching broad band fluorine observation probe (BBFO) with z-gradients. NMR spectra of metal-ligand system were recorded in H_2O-D_2O (90%−10%) solution at 2 mM ligand concentration and different molar ratios by using a stock acidic deuterated aqueous of cadmium chloride and lead nitrate. The pH values have been selected according to those in

which the identified species are present at the maximum concentration based on potentiometric results. The selected metal ion solution was added to the ligand solution and the pH was set just before the spectra acquisition. 2-D $^{1}H–^{13}C$ heteronuclear single quantum coherence spectra (HSQC) were acquired by using a phase-sensitive sequence employing Echo-Antiecho-TPPI gradient selection with a heteronuclear coupling constant JXH = 145 Hz, and shaped pulses for all 180° pulses on f2 channel with decoupling during acquisition; sensitivity improvement and gradients in back-inept were also used (Peana et al., 2015). Relaxation delays of 2 s and 90° pulses of about 10 μs were applied in all experiments. Solvent suppressions were achieved by using excitation sculpting with gradients. All NMR data were processed with TopSpin (Bruker Instruments) software and analyzed by Sparky 3.11 and MestRe Nova 6.0.2 (Mestrelab Research S.L.) programs.

2.2.3. Computational studies

The geometry of Pb^{2+} and Cd^{2+} complexes was fully optimized by DFT calculation using the M06-L (Zhao and Truhlar, 2008) functional and the 6–31 G(d,p) (Francl et al., 1982), (Hariharan and Pople, 1973) basis set. The implicit water solvent effects were evaluated by using the ''conductor-like polarized continuum model'' (CPCM) (Barone and Cossi, 1998). Vibration frequency calculations, within the harmonic approximation, were carried out to estimate the relative standard Gibbs free energy and to confirm that the optimized geometries corresponded to a minimum in the potential energy surface. All the related calculations were performed by the Gaussian 16 program package (Frisch et al., 2019).

3. Results and discussion

The complex formation equilibria of the five ligands with Pb^{2+} and Cd^{2+} have been studied by joined potentiometric-spectrophotometric titrations. The potentiometric data have been processed by HyperQuad program (Gans et al., 1996) taking into account the hydrolysis constants reported in 2.2.1. The spectrophotometric data have been processed by HypSpec program (Gans et al., 1999), although the presence of several differently protonated species did not allow us to consider UV data for calculating stability constants. Despite this, the trend (absorbance *vs* pH) of the two characteristic bands at 268 nm and 314 nm (Fig. S2, Fig. S3) of KA moiety (related to the OH and O^{-} forms respectively) and the chemical shift variation of nuclei F and G have been fundamental for considering the involvement of HPO rings in metal coordination. Furthermore, the spectrophotometric data indicate the starting of precipitation of metal hydroxides, poorly visible to the naked eye, by the raising up of the baseline. Overall, the complexation models have been built up taking into account the protonation constants previously published (Nurchi et al., 2019b), (Nurchi et al., 2018), (Nurchi et al., 2010) (summarized in Table S1) and by the support of NMR spectroscopy and DFT calculation. The complex formation constants and speciation plots are reported in Table 1 and Fig. 2, Fig. 5.

3.1. Lead complexes

3.1.1. Kojic acid

Kojic acid forms Pb^{2+} complexes of two different stoichiometr, $[PbL]^{+}$ and PbL_2: the formation of $[PbL]^{+}$ starts at pH 4 (Fig. 2), reaching 80% of formation at pH 6, when the PbL_2 complex formation begins and rises up to 50% after pH 8. Indeed, the spectra collected during UV titration of Pb^{2+}-KA system at 1:2 metal:ligand molar ratio (Fig. S4, Fig. S5) show the disappearance of the band at 268 nm and the formation of a new one at 306 nm (Fig. S6, Fig. S7). The precipitation of metal hydroxides takes place at pH ~ 10. From pM value (6.57) it follows that at 1 μM concentration of Pb^{2+}, a tenfold excess of ligand complexes the 70% of metal leaving free the remaining 30%, similar to congener maltol (pM 6.76), while deferiprone (7.68) (Buglyó et al., 2015) totally complexes the Pb^{2+} ion.

Table 1
Complex formation constants of Pb^{2+} and Cd^{2+} with KA, S2, S3, S4 and SC ligands evaluated from potentiometric titrations at 25 °C, 0.1 M ionic strength using HyperQuad program (Gans et al., 1996). pM = − $\log_{10}[M_{free}]$ with [M] = 10^{-6} M, [L] = 10^{-5} M and pH = 7.4. L indicates the completely deprotonated form of the ligands (L^{-} for KA, L^{2-} for S2, S3, S4 and L^{3-} for SC). The charges of complexes are omitted for simplicity.

	logβ				
species	KA	S2	S3	S4	SC
$PbLH_4$					46.69(3)
$PbLH_3$			32.73(5)		39.52(1)
$PbLH_2$					31.07(3)
PbLH					22.62(1)
PbL	5.88(3)				12.98(2)
PbL_2	9.85(5)				
$Pb_2L_2H_5$			63.58 (3)	64.86(6)	
$Pb_2L_2H_4$		53.15(8)	56.41 (2)	57.82(3)	
$Pb_2L_2H_3$		45.8(1)	47.92 (2)	48.28(8)	
$Pb_2L_2H_2$		38.88(6)	38.64 (3)	39.43(2)	
Pb_2L_2H		29.9(1)	29.43 (2)		
Pb_2L_2		21.0(6)			
pPb	**6.57**	**6.49**	**6.43**	**6.73**	**10.88**
$CdLH_3$					35.63(5)
$CdLH_2$					28.82(5)
$CdLH_1$					21.55(5)
CdL	4.3(1)				13.89(2)
$CdLH_{-1}$					3.49(3)
CdL_2	8.1(1)				
$Cd_2L_2H_5$			58.9(1)	61.2(1)	
$Cd_2L_2H_4$		50.61(7)	51.1(1)	53.6(1)	
$Cd_2L_2H_3$			42.85(7)	44.43(7)	
$Cd_2L_2H_2$		36.00(5)	33.60(5)	34.6(1)	
Cd_2L_2H		28.15(5)	23.86(4)		
Cd_2L_2		19.96(5)			
$Cd_2L_2H_{-1}$		10.25(6)			
pCd	**6.03**	**6.02**	**6.00**	**6.00**	**7.89**

The ^{1}H and ^{13}C chemical shift difference between Pb^{2+}-KA and KA systems (Fig. S8) confirm the starting of metal complexation at acidic pH showing nuclei F as the most affected due to the involvement of deprotonated phenolic group in coordination.

3.1.2. Kojic acid derivatives

Bis-kojic ligands form binuclear complexes where each of the two Pb^{2+} ions is coordinated by oxygen atoms of the KA moieties of the two different ligands as can be inferred from the trends of the OH and O^{-} groups bands (Fig. S10, Fig. S13, Figs. S16-S18). In particular, the first spectrum of Pb^{2+}-S2 system titration at pH 6.18 (Fig. S10), related to the species $[Pb_2L_2H_4]^{4+}$ (Fig. 2), shows the band of protonated OH groups (276 nm) decreased by ~ 70–80% of absorbance (OH and three amino groups still protonated), which totally disappears in behalf of the band of deprotonated O^{-} groups (308 nm) due to the loss of a proton (pK 7.3) giving $[Pb_2L_2H_3]^{3+}$ species. The following deprotonations occur on the charged amino groups and are spectrally silent. In excess of ligand, also the 1:2 complexes $[PbL_2H_3]^{+}$ and PbL_2H_2 take place. NMR spectra were collected at pH 7.68 increasing the Pb^{2+} concentration up to 1:1 metal: ligand molar ratio (Fig. 3). The Pb^{2+}-S2 system is characterized by a fast exchange rate: adding stoichiometric amount of Pb^{2+} to the ligand, the ^{1}H NMR signals progressively shift and appear to be averaged among the S2 free and bound exchanging states. In the whole pH range, the major perturbation is related to the F nuclei (Fig. 3), closest to the coordinating O^{-} groups, followed by G ≥ E > > D confirming the coordination by the oxygen donors of kojic units, whereas the nitrogen donors are excluded in the complex formation. By increasing pH above 9, the ligand does not appear influenced by the metal ion since it is involved in hydroxides formation/precipitation.

To obtain atomistic models of the binuclear Pb^{2+} complexes, DFT calculations have been performed on the hypothesized structures reported in Fig. 4, considering the protonation states $[Pb_2(S2)_2H]^{+}$,

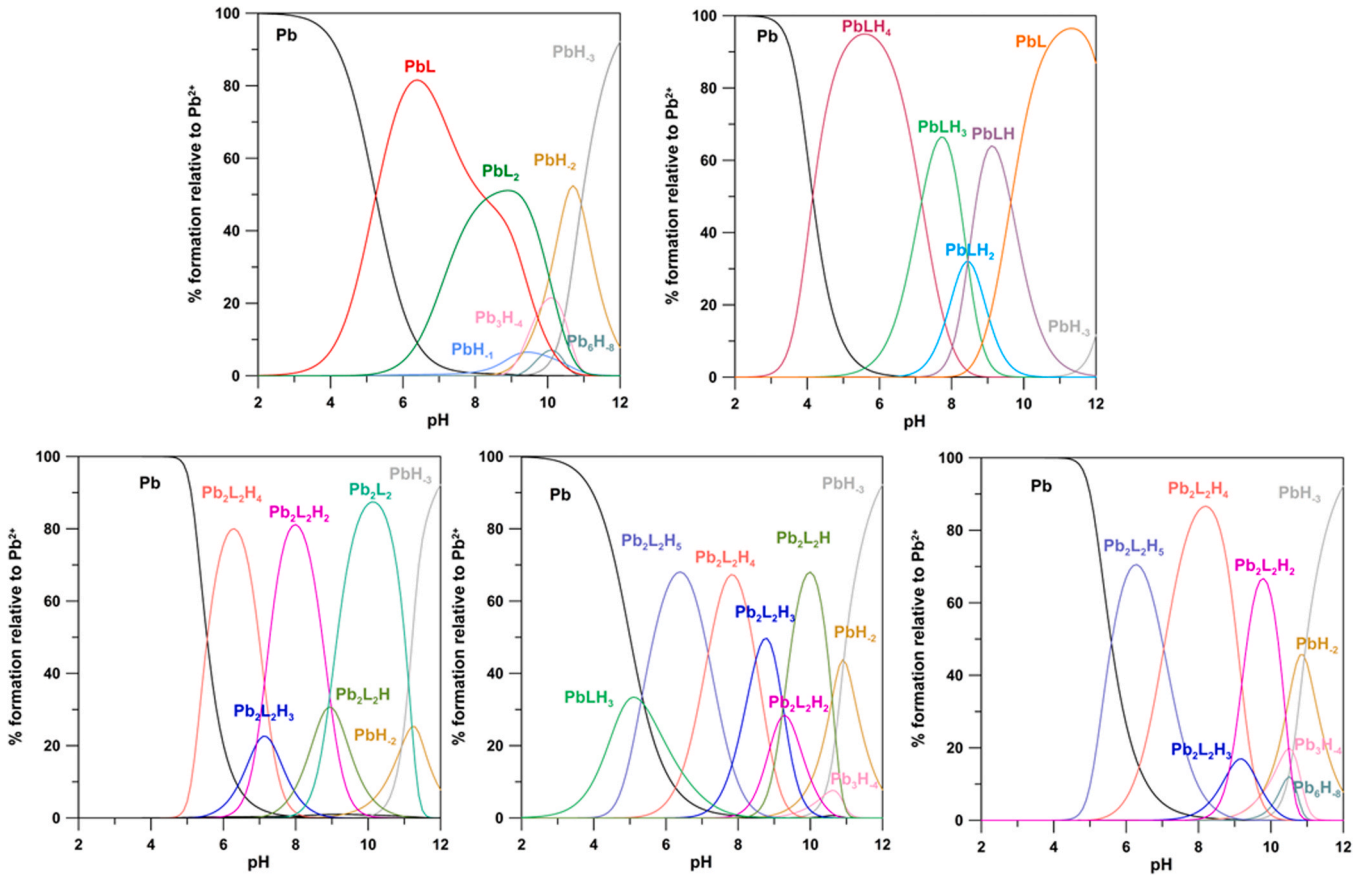

Fig. 2. Speciation plots of Pb^{2+}-ligand systems calculated with Hyss program (Alderighi et al., 1999) at 5.0×10^{-4} M ligand concentration and at 1:2 metal:ligand molar ratio for KA ligand and 1:1 for S2, S3, S4 and SC ligands. Top): from left to right KA and SC ligands; bottom): from left to right S2, S3 and S4 ligands.

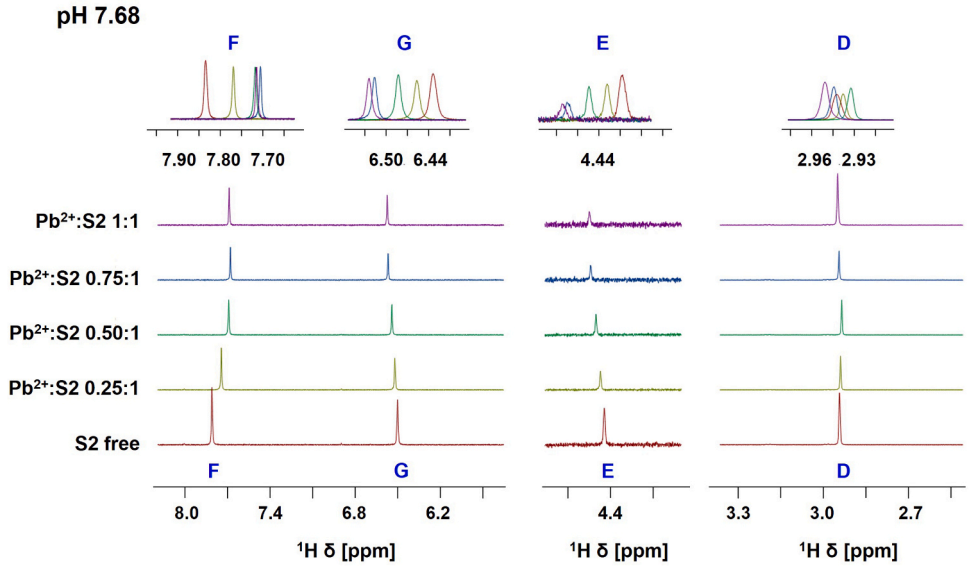

Fig. 3. ^{1}H NMR spectra of Pb^{2+}-S2 system at different molar ratios and pH 7.68.

$[Pb_2(S2)_2H_2]^{2+}$ and $[Pb_2(S2)_2H_3]^{3+}$. The results obtained show that each of the two S2 ligands binds both metal ions through the two chelating oxygen units in KA moieties. Furthermore, only one oxygen atom of each S2 ligand is bridging both metal ions. Ligand protonation involves the four amine groups of the two S2 ligands.

A different scheme has to be assumed at the starting of complexation by S3 ligand: in $[PbLH_3]^{3+}$ complex Pb^{2+} is bound to one KA unit, being the second still protonated, as well as the two nitrogen atoms in the linker. The joining of two $[PbLH_3]^{3+}$ complexes gives rise to a binuclear $[Pb_2L_2H_5]^{5+}$ (Fig. 2) complex (structurally similar to the $[Pb_2L_2H_4]^{4+}$ with S2), being however protonated on all the four amino groups. Analogously to what observed with S2 ligand, a proton is lost from the

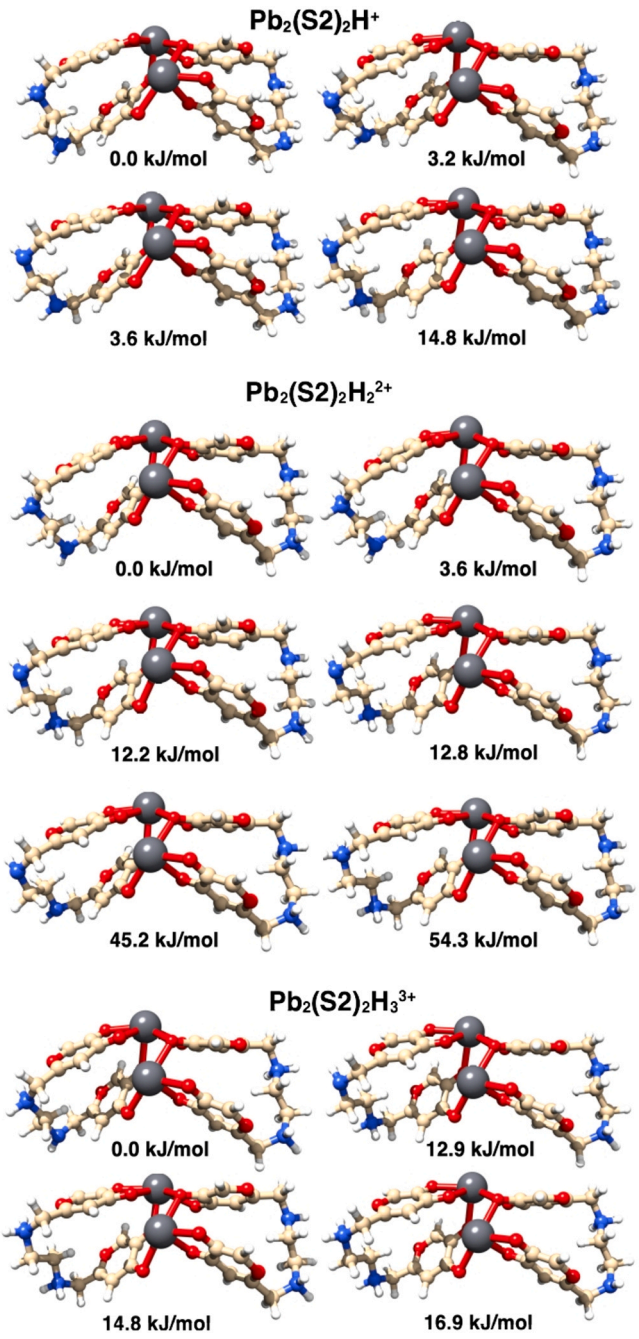

Fig. 4. Structures of the most stable tautomers in water solution, and relative Gibbs free energy values, obtained by DFT calculations of the binuclear Pb^{2+} complexes with top): $S2^{2-}$ and $HS2^{-}$ ligands, in bridge coordination; middle): two $HS2^{-}$ or H_2S2 and $S2^{2-}$ ligands, in bridge coordination; bottom): with H_2S2 and $HS2^{-}$ ligands, in bridge coordination.

last uncoordinated KA moiety with pK 7.17, with the formation of $[Pb_2L_2H_4]^{4+}$, and the further protons are lost in the pK range 8.48–9.28 until the formation of the $[Pb_2L_2H]^{+}$ complex. S4 ligand gives a complexation model analogous to that of S3 ligand, completing Pb^{2+} coordination with the loss of a proton with pK 7.04 from $[Pb_2L_2H_5]^{5+}$ (Fig. 2). The NMR behavior of both S3 (Fig. S14) and S4 (Fig. S19) ligands looks similar to that of S2. In all systems, the metal interaction starts at ~ pH 5 involving the oxygen donor atoms of KA units until ~ pH 9.

Regarding the tris-kojic ligand SC, a mononuclear species $[PbLH_4]^{3-}$ starts to form before pH 4, where Pb^{2+} is presumably coordinated by two KA units (being the third still protonated as well as the three nitrogen atoms of the linker). Spectrophotometric data (Fig. S21, Fig. S23) give evidence that the first proton is lost from KA, since the deprotonation take place at pK 7.2, as in the free ligand. The following three protons are lost at 8.4–9.6 pK range, slightly lower than those of the free ligand. The trend of the chemical shifts variation is analogous to the previously described systems (Fig. S11) indicating that the metal ion binding involves the chelating oxygen atoms of the KA units. The structure of the Pb^{2+} complexes have been investigated by DFT calculations, (hypothesized structures in Figs. S24-S26) considering the protonation states $[Pb(SC)]^{-}$, $[Pb(SC)H]$, $[Pb(SC)H_2]^{+}$, $[Pb(SC)H_3]^{2+}$, and $[Pb(SC)H_4]^{3+}$. Independently of the complex overall charge, preferential metal coordination always occurs through the chelating phenolic oxygen atoms of the KA units.

3.2. Cadmium complexes

3.2.1. Kojic acid

Kojic acid forms 1:1 complex at pH > 5, $[CdL]^{+}$, and 1:2 complex after pH 6, CdL_2. Their stoichiometry and the related stability constants are in agreement with those reported in the literature (Kotani et al., 1976), (Pecsok, 1961). From the trend of the perturbations *vs* pH identified by NMR spectra (Fig. S31), it appears that the interaction of Cd^{2+} with KA is more complicated due to the presence of different species in solution, but substantially in agreement with potentiometric results. All species involve KA unit oxygen donors. A decrease in chemical shift perturbations is observed at pH > 10, associated with the formation of hydroxylated species that causes the precipitation of the metal and the re-formation of free KA.

3.2.2. Kojic acid derivatives

Although bis-kojic ligands form Cd^{2+} complexes with the same stoichiometry of Pb^{2+} complexes, the spectral behavior of the studied systems do not necessary imply the involvement of KA moieties in the metal ion coordination. S2 ligand gives $[Cd_2L_2H_4]^{4+}$ complex (as with Pb^{2+}) as first formed species, which loses its four proton and a fifth one from a coordinated water molecule (it cannot be assigned to a particular deprotonation step) in the 7.3–9.7 pH range. Differently from what observed for Pb^{2+} complexes, the spectrophotometric data (Fig. S33, Fig. S35) show that the characteristic band of deprotonated O^{-} groups (316 nm) is formed in a small extent, implying that Cd^{2+} is only partially coordinated by KA. Namely, from NMR spectra collected at pH 7.84 increasing the Cd^{2+} concentration up to 1:1 metal:ligand molar ratio (Fig. 6) and from chemical shift variation in the wide pH range (Fig. S36), the trend of ^{1}H signals follows the order G > > F (opposite to the Pb^{2+} complexation) and the perturbation of D and E nuclei is more consistent than that given in Pb^{2+} complexation. It may indicate that, for some species in solution, the nitrogen donors of the linker could be involved in the metal interaction. DFT calculations have been performed on $[Cd_2(S2)_2H]^{+}$, $[Cd_2(S2)_2H_2]^{2+}$ and $[Cd_2(S2)_2H_3]^{3+}$, using the same stoichiometry and coordination scheme of the Pb^{2+} complexes of ligand S2, (Fig. S37). The results obtained support the occurrence of analogous species in solution.

The S3 and S4 ligands present a similar behavior (Figs. S39-S41, Figs. S44-S46). The first formed species is $[Cd_2L_2H_5]^{5+}$ for both of them, witch lose their protons till the formation of $[Cd_2L_2H]^{+}$ for S3, and of $[Cd_2L_2H_2]^{2+}$ for S4. However, the implication of KA moieties in Cd^{2+} coordination is evident from the band at 266 nm (Fig. S39, Fig. S44). Conversely, to S2 complexes, for S3 and S4 ligands, the major chemical shift variations are detected only for G and F nuclei, while D and E ones are blandly affected. Consequently, it seems that the nitrogen donor atoms do not take part in the coordination (Fig. S42, Fig. S47). Cd^{2+} mononuclear complexes are formed even with SC ligand. $[CdLH_3]^{2+}$ complex loses sequentially four protons till the formation of the hydroxo $[CdLH_{-1}]^{2-}$ complex, where KA units are not involved in the Cd^{2+} coordination, according to the spectrophotometric data (Figs. S49-S51).

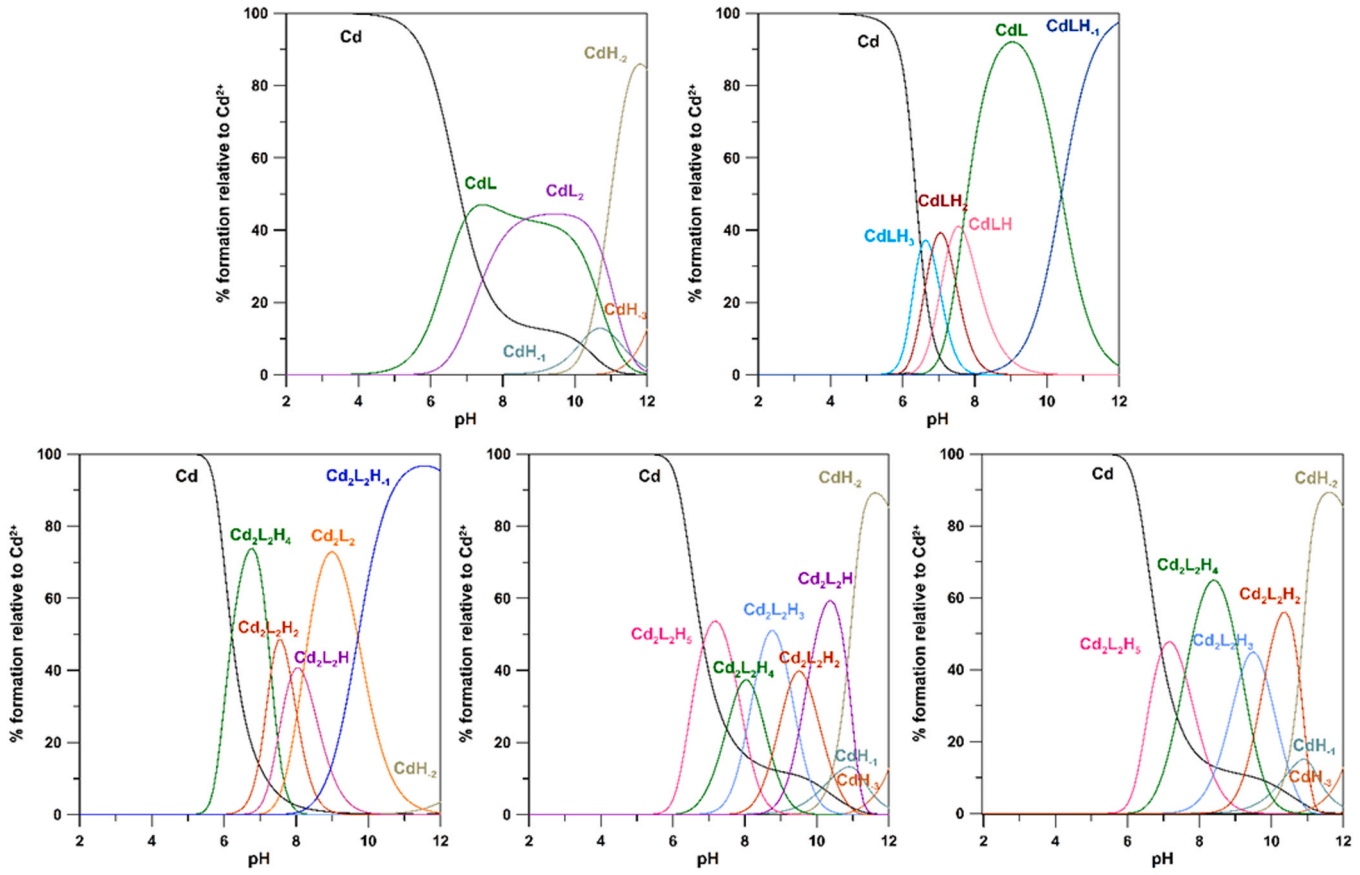

Fig. 5. Speciation plots of Cd^{2+}-ligand systems calculated with Hyss program (Alderighi et al., 1999) at 5.0×10^{-4} M ligand concentration and at 1:2 metal:ligand molar ratio for KA ligand and 1:1 for S2, S3, S4 and SC ligands Top): from left to right KA and SC ligands. Bottom): from left to right S2, S3 and S4 ligands.

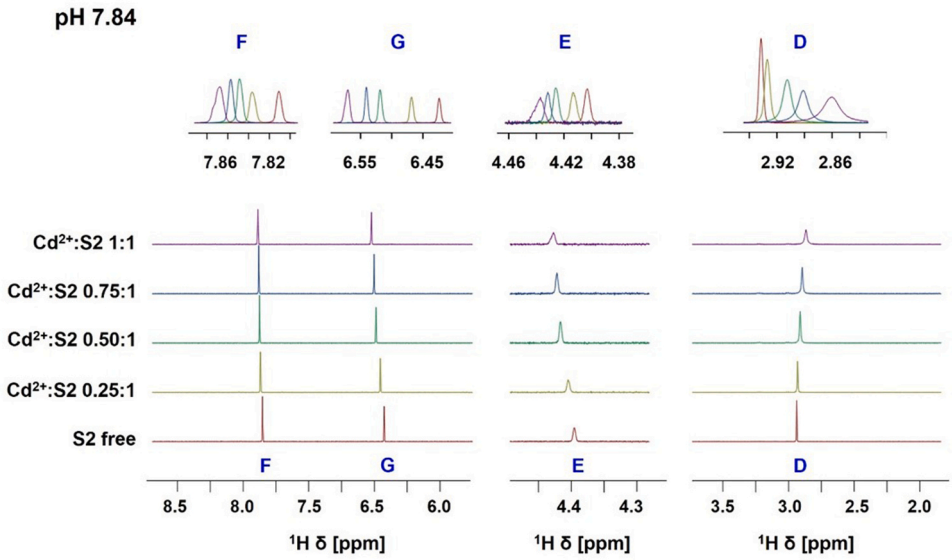

Fig. 6. ^{1}H NMR spectra of Cd^{2+}-S2 system at different molar ratios and pH 7.84.

Moreover, as it clearly appears from Fig. S36, D and C are the most affected nuclei at pH 6.6, before which (pH 5.74) no metal interaction is observed (in agreement with potentiometric data). The trend of chemical shift variation is fairly kept constant up to pH 8, suggesting the presence of one predominant species or a similar species in solution. From pH 8 onwards, there is a gradual variation of the trend which leads to a new species at high pH value (pH 10.9) proposing the involvement of the nitrogen donor atoms in Cd^{2+}-SC complexes. The presence of two separate peaks in (Fig. S52), one related to SC in free conformation and the second related to Cd^{2+}-SC conformation), suggest a slow exchange in NMR timescale and a high affinity Cd^{2+} binding.

Interestingly, DFT calculations point out the occurrence of a fundamental difference between lead and cadmium complexes of ligand SC. In fact, while for $[Cd(SC)]^{-}$ (Fig. S53), preferential metal coordination

occurs through the oxygen atoms of the three KA units, for the protonated $[Cd(SC)H_3]^{2+}$ form the most stable species shows the preferential coordination through the four amine nitrogen atoms of the ligand.

3.3. S ligands in Pb^{2+} and Cd^{2+} remediation

A quantitative evaluation of S ligands as chelating agents in Pb^{2+} and Cd^{2+} remediation was made using the stability constants reported in Table 1.

Firstly, the behavior of the two metal ions towards each one of ligands was investigated through the correlation between logβ of the most protonated Cd^{2+} complex and logβ of Pb^{2+} complex of the same stoichiometry. The linear trend in Fig. 7 (regression equation $y = 0.961x - 1.529$ and $R^2 = 0.9988$) implies that the stability of Cd^{2+} complexes in S ligands is definitely lower than the corresponding one of Pb^{2+} complexes.

To compare these findings with the general behavior of Pb^{2+} and Cd^{2+} complexes, the complex formation constants (Pettit and Powell, 2001) of these two metal ions with ten ligands characterized by carboxylic, amino and mercapto groups were taken into account, limiting to values at 25 °C and 0.1 M ionic strength, and to stability constants for each ligand measured by the same authors (Table S2). A linear correlation was found also in this case. The difference of the related regression line $y = 0.931x - 0.528$ (Fig. 7 right) from the previous one $y = 0.961x - 1.529$ (Fig. 7 left) can be ascribed to the limited number of experimental points; at any rate, the calculated decrease of Cd^{2+} constants with respect to those of Pb^{2+}, calculated with both equations, is almost the same due to the mutual compensation between y-intercept and slope contributions.

As a final point, the trend of the percent concentration of free metal ion and of total complexed metal ion *vs* pH was evaluated (Fig. 8). The percent concentration of complexed metal ion has to be assumed as the contribution of all species (Fig. 2, Fig. 5) for each metal ion-ligand system. Contrary to the aminopolycarboxylic acids (Nurchi et al., 2020) that form metal complexes of simple 1:1 stoichiometry, the proposed S ligands form complexes differing in stoichiometry and protonation degree. Therefore, the total complexed metal ion *vs* pH is of extreme utility in the quantitative evaluation of the ligand binding capacity.

Additive information are presented in S.I., i.e. the pPb and pCd values for S ligands and for aminopolycarboxylic acids (Table S3), and the pH values at which given percent's of complexation occur (Table S4).

The obtained data show a limited applicability of S2, S3 and S4 ligands for remediation with respect to aminopolycarboxylic acids. This has to be ascribed to the different properties of coordinating oxygen groups in the two class of ligands: coordinating O^- groups in the KA units, despite their capacity to coordinate Pb^{2+} and Cd^{2+} ions, present protonation constants 4–6 log K units higher than those of carboxylic groups in aminopolycarboxylic acids. This feature determines a strong competition between protons and metal cations toward the same chelating groups in S ligands. Completely different situation is shown by SC ligand. Actually, it forms strong complexes with both Pb^{2+} and Cd^{2+}, characterized by high pM values (10.88 and 7.89 respectively).

The pM values reported in Table 1 allow some consideration on the remediation capacity of the studied ligands in the treatment of wastewater. These values are calculated on solutions containing a starting 1 μM concentration of the toxic metal ions, which correspond to 207 μg L^{-1} for Pb^{2+} and 112 μg L^{-1} for Cd^{2+}. These concentrations are extremely higher than the threshold limits in drinking water of 5 μg L^{-1} for both metal ions according US legislation (ATSDR, 2021), (ATSDR, 2013) and of 10 μg L^{-1} for Pb^{2+} and 3 μg L^{-1} for Cd^{2+} according (WHO, 2017). The calculated pM values correspond to the concentration of free metal ion after the addition of a tenfold excess of ligand. In the case of the Pb^{2+} the 6.43 pM with S3 (the lowest value) corresponds to a drop of concentration of free Pb^{2+} from 207 to 77 μg L^{-1} after ligand addition, the 6.73 pM with S4 from 207 to 39 μg L^{-1}, and 10.88 pM for SC to correspond to a drop from 207 to 0.003 μg L^{-1} (99.999% of decrease). Then, even if an amount of free metal ion ranging from 60% to 80% is removed by KA, S2, S3 and S4, these ligands are unable to carry the concentration into the legal limits. On the contrary, SC is extremely efficacious in producing pure water from a high-polluted solution. In the case of Cd^{2+}, all the ligands are unable to reduce the metal ion concentration in a remarkable amount, while SC also in this case is efficacious in carrying the polluted solution into the requested values of concentration.

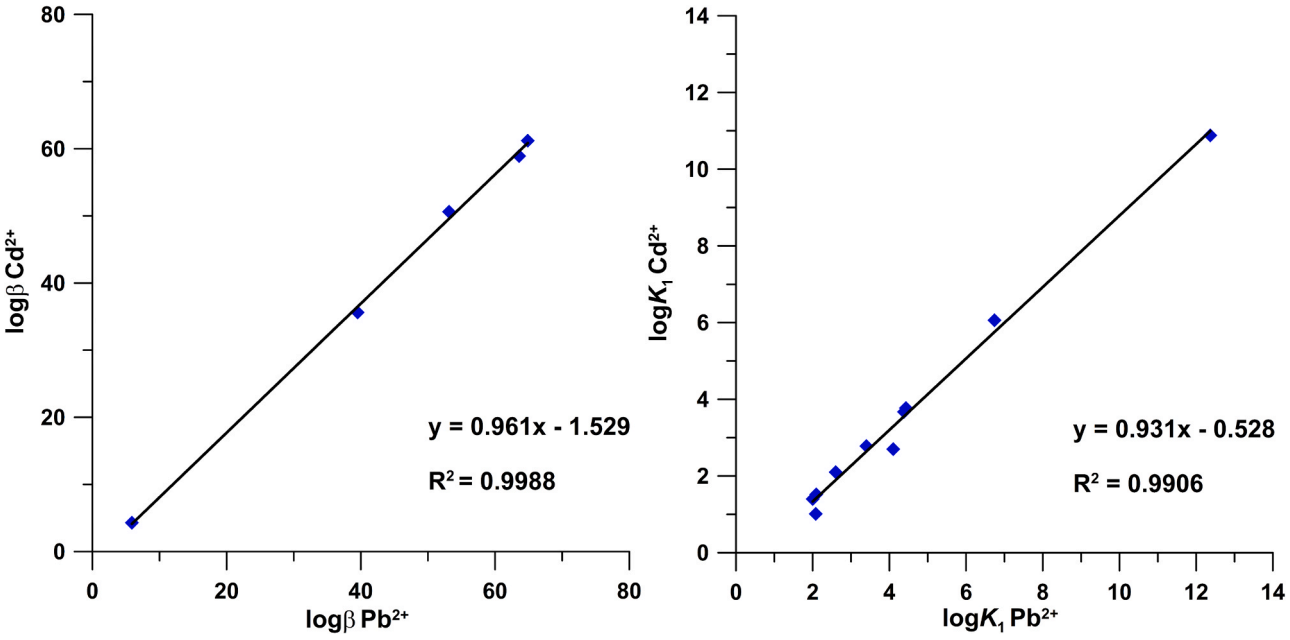

Fig. 7. Left): Logβ of the most protonated Cd^{2+} complex vs Logβ of the most protonated Pb^{2+} complex for each S ligand: logβ (CdL) = 4.33 vs logβ (PbL) = 5.88 for KA; logβ ($Cd_2L_2H_4$) = 50.61 vs logβ ($Pb_2L_2H_4$) = 53.15 for S2; logβ ($Cd_2L_2H_5$) = 58.9 vs logβ ($Pb_2L_2H_5$) = 63.58 for S3; logβ ($Cd_2L_2H_5$) = 61.2 vs logβ ($Pb_2L_2H_5$) = 64.86 for S4; logβ ($CdLH_3$) = 35.63 vs logβ ($PbLH_3$) = 39.52 for SC. Right): $LogK_1$ Cd^{2+} complex vs $LogK_1$ Pb^{2+} complex for selected ligands (Table S2).

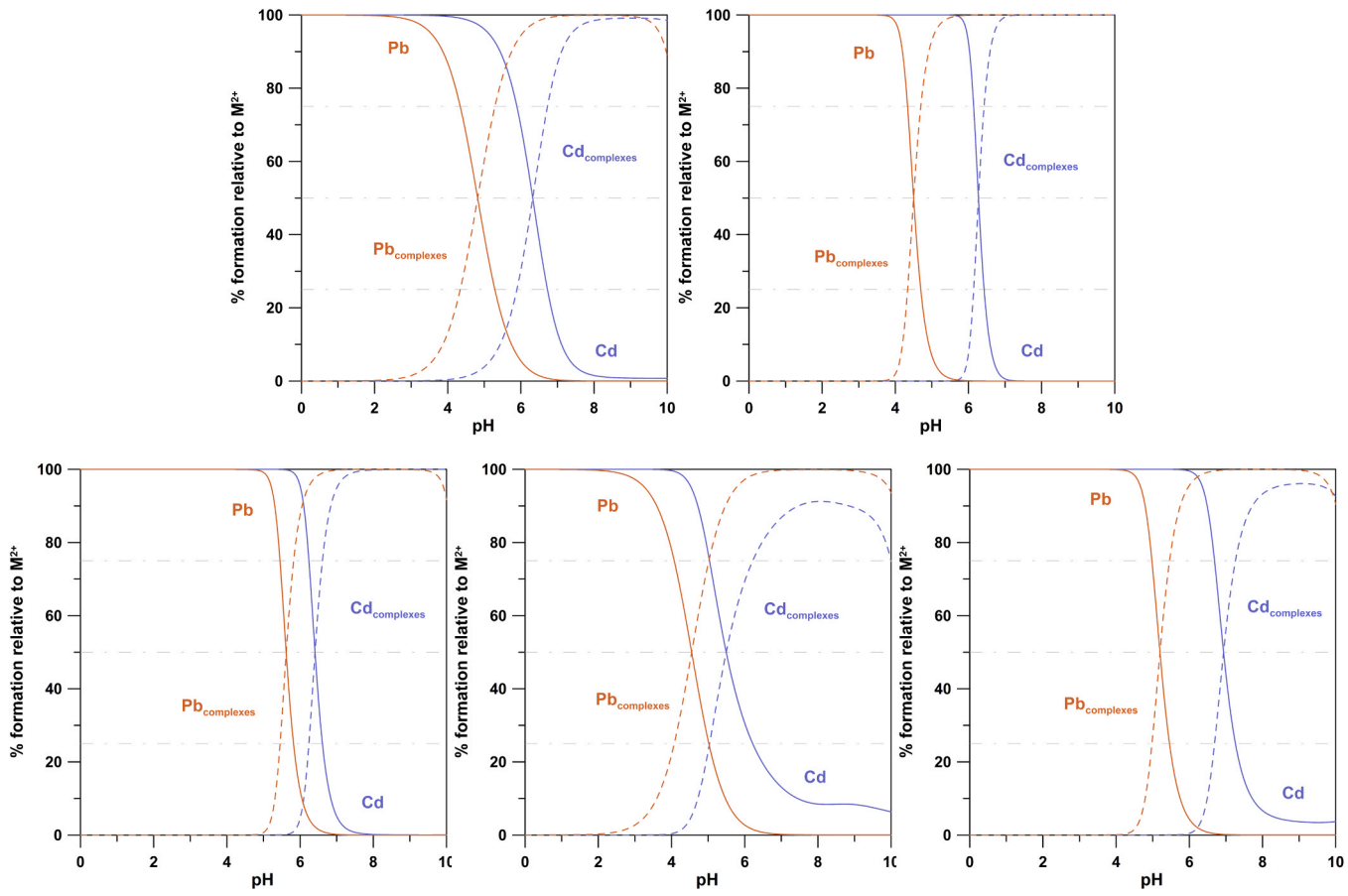

Fig. 8. Percent concentration of free metal ion and total complexed metal ion at different pH assuming the complexed metal ion as the contribution of all species for each metal-ligand system. (i.e. for Pb^{2+}-SC system, % concentration of Pb^{2+}complexes = % concentration of $PbLH_4 + PbLH_3 + PbLH_2 + PbLH + PbL$). Top): from left to right KA and SC ligands. Bottom): from left to right S2, S3 and S4 ligands. Solid line and dashed line indicate free metal ion and complexed metal ion respectively. Gride lines point out the 25%, 50%, 75% of complex formation.

4. Conclusions

Some concluding considerations can be drawn on the results obtained remarking the most interesting findings. Experimental and DFT calculations highlight the different coordination mechanism toward Pb^{2+} and Cd^{2+}: in the case of Pb^{2+}, coordination takes place exclusively via the oxygen atoms in the KA units, while in the case of Cd^{2+} the contribute of the nitrogen atoms in the linker appears significant.

As far as the complex formation constants are concerned, all the studied ligands form complexes of significantly stronger stability with Pb^{2+} than with Cd^{2+}. The stability of SC complexes is higher of different magnitude orders respect to those obtained with all other ligands. These findings influence the possible application of the proposed ligands in soil and water remediation. The proposed numerical cases show that at proper pH values all the S ligands can be used for decorporation of polluted soils from Pb^{2+}, but only SC ligand can find applications in the case of Cd^{2+}. For polluted waters, the use of a tenfold excess of S2, S3 and S4 ligands can reduce in a large amount the concentration of Pb^{2+}, within the law limits for the discharge of wastewater into surface water systems, but it is not able to bring it within the limits for drinking water. SC ligand allows instead the complete removal of lead from water. In the case of Cd^{2+} only SC ligands can find applications for water treatment. Into the outlined limits, the utilization of S ligands in the free form, or anchored on a solid support, is surely promising, and request further studies for determining the conditions of real use.

CRediT authorship contribution statement

Rosita Cappai: Conceptualization, Methodology, Formal analysis, Investigation, Data curation, Writing – original draft, Writing – review & editing, Supervision. **Alessandra Fantasia:** Formal analysis, Investigation, Writing – original draft. **Giampaolo Barone:** Validation, Formal analysis, Data curation. **Massimiliano F. Peana:** Validation, Data curation. **Alessio Pelucelli:** Investigation, Methodology. **Serenella Medici**: Conceptualization, Writing – review & editing. **Guido Crisponi:** Validation, Data curation, Writing – review & editing. **Valeria M. Nurchi:** Writing – original draft, Writing – review & editing, Funding acquisition, Resources. **Maria Antonietta Zoroddu:** Writing – original draft, Writing – review & editing, Funding acquisition, Resources.

Declaration of Competing Interest

The authors declare that they have no known competing financial interests or personal relationships that could have appeared to influence the work reported in this paper.

Data availability

Data will be made available on request.

Acknowledgements

This work was supported by Regione Autonoma Sardegna [RASSR79857], Fondazione di Sardegna [CUP F72F20000240007],

Fondo di Ateneo per la Ricerca [2019,2467], Fondo di Ateneo per la Ricerca [2020,2465], CINECA award [IsC93, 2021], NECTAR, by COST (European Cooperation in Science and Technology) [CA18202].

Appendix A. Supporting information

Supplementary data associated with this article can be found in the online version at doi:10.1016/j.ecoenv.2023.115470.

References

Agency for Toxic Substances and Disease Registry., 2012. ⟨https://wwwn.cdc.gov/TSP/ToxProfiles/ToxProfiles.aspx?id=48&tid=15⟩. (Accessed May 19, 2023).

Agency for Toxic Substances and Disease Registry., 2013. ⟨https://www.atsdr.cdc.gov/csem/cadmium/Safety-Standards.html⟩. (Accessed Jan 26, 2023).

Agency for Toxic Substances and Disease Registry., 2020. ⟨https://wwwn.cdc.gov/TSP/ToxProfiles/ToxProfiles.aspx?id=96&tid=22⟩. (Accessed May 19, 2023).

Agency for Toxic Substances and Disease Registry., 2021. ⟨https://www.atsdr.cdc.gov/csem/leadtoxicity/safety_standards.html⟩. (Accessed Jan 26, 2023).

Agency for Toxic Substances and Disease Registry., 2022. ⟨https://www.atsdr.cdc.gov⟩. (Accessed Jan 26, 2023).

Alderighi, L., Gans, P., Ienco, A., Peters, D., Sabatini, A., Vacca, A., 1999. Hyperquad simulation and speciation (HySS): a utility program for the investigation of equilibria involving soluble and partially soluble species. Coord. Chem. Rev. 184, 311–318.

Baes, C.F., Mesmer, R.S., 1976. The Hydrolysis of Cations. John Wiley & Sons,, New York.

Barone, V., Cossi, M., 1998. Conductor solvent model. J. Phys. Chem. A 102, 1995–2001.

Bjørklund, G., Crisponi, G., Nurchi, V.M., Cappai, R., Djordjevic, A.B., Aaseth, J., 2019. A review on coordination properties of thiol-containing chelating agents towards mercury, cadmium, and lead. Molecules 24, 1–32.

Buglyó, P., Bíró, L., Nagy, I., Szocs, B., Farkas, E., 2015. Hydroxypyronate, thiohydroxypyronate and hydroxypyridinonate derivatives as potential Pb^{2+} sequestering agents. Polyhedron 92, 7–11.

Cantu, J., Valle, J., Flores, K., Gonzalez, D., Valdes, C., Lopez, J., Padilla, V., Alcoutlabi, M., Parsons, J., 2019. Investigation into the thermodynamics and kinetics of the binding of Cu^{2+} and Pb^{2+} to TiS_2 nanoparticles synthesized using a solvothermal process. J. Environ. Chem. Eng. 7, 103463–103473.

Cappai, R., Chand, K., Lachowicz, J.I., Chaves, S., Gano, L., Crisponi, G., Nurchi, V.M., Peana, M., Zoroddu, M.A., Santos, M.A., 2018. A new tripodal-3-hydroxy-4-pyridinone for iron and aluminium sequestration: synthesis, complexation and: In vivo studies. New J. Chem. 42, 8050–8061.

Cardiano, P., Foti, C., Giuffrè, O., 2016. On the interaction of N-acetylcysteine with Pb^{2+}, Zn^{2+}, Cd^{2+} and Hg^{2+}. J. Mol. Liq. 223, 360–367.

Crisponi, G., Nurchi, V., 2015. Metal Ion Toxicity. In: Encyclopedia of Inorganic and Bioinorganic Chemistry. John Wiley & Sons, Ltd (Eds.).

Francl, M.M., Pietro, W.J., Hehre, W.J., Binkley, J.S., Gordon, M.S., DeFrees, D.J., Pople, J.A., 1982. Self-consistent molecular orbital methods. XXIII. A polarization-type basis set for second-row elements. J. Chem. Phys. 77, 3654–3665.

Frassineti, C., Ghelli, S., Gans, P., Sabatini, A., Moruzzi, M.S., Vacca, A., 1995. Nuclear magnetic resonance as a tool for determining protonation constants of natural polyprotic bases in solution. Anal. Biochem. 231, 374–382.

Frisch, M.J., Trucks, G.W., Schlegel, H.B., Scuseria, G.E., Robb, M.A., Cheeseman, J.R., Scalmani, G., Barone, V., Mennucci, B., Petersson, G.A., Nakatsuji, H., Caricato, M., Li, X., Hratchian, H.P., Izmaylov, A.F., Bloino, J., Zheng, G., Sonnenberg, J.L., 2019. Gaussian Inc., Wallingford, CT.

Gans, P., Sabatini, A., Vacca, A., 1996. Investigation of equilibria in solution. Determination of equilibrium constants with the HYPERQUAD suite of programs. Talanta 43, 1739–1753.

Gans, P., Sabatini, A., Vacca, A., 1999. Determination of equilibrium constants from spectrophotometric data obtained from solutions of known pH: the program pHab. Ann. Chim. 89, 45–50.

Gran, G., 1952. Determination of the equivalence point in potentiometric acid-base titrations. Analyst 77, 661–671.

Hariharan, P.C., Pople, J.A., 1973. The influence of polarization functions on molecular orbital hydrogenation energies. Theor. Chim. Acta 28, 213–222.

Irto, A., Cardiano, P., Chand, K., Cigala, R.M., Crea, F., De Stefano, C., Gano, L., Gattuso, G., Sammartano, S., Santos, M.A., 2019. A new bis-(3-hydroxy-4-pyridinone)-DTPA-derivative: synthesis, complexation of di-/tri-valent metal cations and in vivo M^{3+} sequestering ability. J. Mol. Liq. 281, 280–294.

Irto, A., Cardiano, P., Chand, K., Cigala, R.M., Crea, F., De Stefano, C., Gattuso, G., Sammartano, S., Santos, M.A., 2020. Complexation of environmentally and biologically relevant metals with bifunctional 3-hydroxy-4-pyridinones. J. Mol. Liq. 319, 114349–114368.

Kotani, T., Ichimoto, I., Tatsumi, C., Fujita, T., 1976. Bacteriostatic activities and metal chelation of kojic acid analogs. Agric. Biol. Chem. 40, 765–770.

Nurchi, V.M., Crisponi, G., Lachowicz, J.I., Murgia, S., Pivetta, T., Remelli, M., Rescigno, A., Niclós-Gutíerrez, J., González-Pérez, J.M., Domínguez-Martín, A., Castiñeiras, A., Szewczuk, Z., 2010. Iron(III) and aluminum(III) complexes with hydroxypyrone ligands aimed to design kojic acid derivatives with new perspectives. J. Inorg. Biochem. 104, 560–569.

Nurchi, V.M., Crisponi, G., Lachowicz, J.I., Jaraquemada-Pelaez, M. de G., Bretti, C., Peana, M., Medici, S., Zoroddu, M.A., 2018. Equilibrium studies of new bis-hydroxypyrone derivatives with Fe^{3+}, Al^{3+}, Cu^{2+} and Zn^{2+}. J. Inorg. Biochem. 189, 103–114.

Nurchi, V.M., Crisponi, G., Sanna, G., Pérez-Toro, I., Niclos-Gutierrez, J., Gonzalez-Perez, M.J., Domínguez Martín, A., 2019a. Complex formation equilibria of polyamine ligands with copper(II) and zinc(II). J. Inorg. Biochem. 194, 26–33.

Nurchi, V.M., de Guadalupe Jaraquemada-Pelaez, M., Crisponi, G., Lachowicz, J.I., Cappai, R., Gano, L., Santos, M.A., Melchior, A., Tolazzi, M., Peana, M., Medici, S., Zoroddu, M.A., 2019b. A new tripodal kojic acid derivative for iron sequestration: synthesis, protonation, complex formation studies with Fe^{3+}, Al^{3+}, Cu^{2+} and Zn^{2+}, and in vivo bioassays. J. Inorg. Biochem. 193, 152–165.

Nurchi, V.M., Cappai, R., Crisponi, G., Sanna, G., Alberti, G., Biesuz, R., Gama, S., 2020. Chelating agents in soil remediation: a new method for a pragmatic choice of the right chelator. Front. Chem. 8, 1–10.

Nurchi, V.M., Cappai, R., Spano, N., Sanna, G., 2021. A friendly complexing agent for spectrophotometric determination of total iron. Molecules 26, 1–11.

Peana, M., Medici, S., Nurchi, V.M., Lachowicz, J.I., Crisponi, G., Crespo-Alonso, M., Santos, M.A., Zoroddu, M.A., 2015. An NMR study on the 6,6′-(2-(diethylamino) ethylazanediyl)bis(methylene)bis(5-hydroxy-2-hydroxymethyl-4H-pyran-4-one) interaction with A(III) and Zn(II) ions. J. Inorg. Biochem. 148, 69–77.

Peana, M., Pelucelli, A., Medici, S., Cappai, R., Nurchi, V.M., Zoroddu, M.A., 2021. Metal toxicity and speciation: a review. Curr. Med. Chem. 28, 7190–7208.

Pearson, R.G., 1963. Hard and soft acids and bases. J. Am. Chem. Soc. 85, 3533–3539.

Pecsok, R.L., Meeker, R.L., Shields, L.D., 1961. Chelates of cadmium with kojic acid. J. Am. Chem. Soc. 83, 2081–2085.

Pettit, L.D., Powell, K.J., 2001. The IUPAC Stability Constants Database 5.7. Academic Software Timble,, Otley, Yorks, UK.

Remelli, M., Nurchi, V.M., Lachowicz, J.I., Medici, S., Zoroddu, M.A., Peana, M., 2016. Competition between Cd(II) and other divalent transition metal ions during complex formation with amino acids, peptides, and chelating agents. Coord. Chem. Rev. 327–338, 55–69.

World Health Organization, 2017. Guidelines for drinking-water quality: fourth edition incorporating the first addendum. Geneve. ⟨https://www.who.int/publications/i/item/9789241549950⟩ (Accessed Jan 26, 2023).

Zhao, Y., Truhlar, D.G., 2008. The M06 suite of density functionals for main group thermochemistry, thermochemical kinetics, noncovalent interactions, excited states, and transition elements: two new functionals and systematic testing of four M06-class functionals and 12 other function. Theor. Chem. Acc. 120, 215–241.